Biogeosciences Discuss., 9, 17975–17997, 2012
www.biogeosciences-discuss.net/9/17975/2012/
doi:10.5194/bgd-9-17975-2012

Biogeosciences Discussions

Intrusion of coastal waters into the pelagic Eastern Mediterranean: in situ and satellite-based characterization

S. Efrati[1], Y. Lehahn[2,3], E. Rahav[4], N. Kress[5], B. Herut[5], I. Gertman[5], R. Goldman[5], T. Ozer[5], M. Lazar[1], and E. Heifetz[2,6]

[1]The Dr. Moses Strauss Department of Marine Geosciences, University of Haifa, Mt. Carmel, 31905, Israel
[2]Dept. of Geophysics and Planetary Sciences, Tel Aviv University, Ramat Aviv 69978, Israel
[3]Dept. of Environmental Sciences, Weizmann Institute, Rehovot 76100, Israel
[4]Mina and Everard Goodman Faculty of Life Sciences, Bar-Ilan University, Ramat Gan 52900, Israel
[5]Israel Oceanographic Limnological Research, The National Institute of Oceanography, P.O. Box 8030, Tel Shikmona, Haifa 31080, Israel
[6]Dept. of Meteorology, Stockholm University, Sweden

Received: 22 October 2012 – Accepted: 22 Novermber 2012 – Published: 13 December 2012

Correspondence to: Y. Lehahn (yoav.lehahn@weizmann.ac.il),
S. Efrati (shai.efrati@mail.huji.ac.il)

Published by Copernicus Publications on behalf of the European Geosciences Union.

Abstract

A combined dataset of near real time multi-satellite observations and in situ measurements from a high-resolution survey, is used for characterizing physical-biogeochemical properties of a patch stretching from the coast to the open sea in the Levantine basin of the Eastern Mediterranean. Spatial analysis of the combined dataset indicates that the patch is a semi-enclosed system, bounded within the mixed layer and separated from ambient waters by transport barriers induced by horizontal stirring. As such, the patch is characterized by physical-biogeochemical properties that significantly differ from those of the waters surrounding it, with lower salinity, higher temperatures, higher concentrations of silicic acid and chlorophyll *a*, and higher abundance of Synechococcus and Picoeukaryotes cells. Based on estimates of patch dimensions (~ 40 km width and ~ 25 m depth) and propagation speed (~ 0.09 m s^{-1}), the volume flux associated with the patch is found to be in the order of 0.1 Sv. Our observations suggest that horizontal stirring by surface currents is likely to have an important impact on the ultra-oligotrophic Levantine basin ecosystem, through (1) transport of nutrients and coastal derived material, and (2) formation of local, dynamically isolated, niches. In addition, this work provides a satellite-based framework for planning and executing high resolution sampling strategies in the interface between coast and the open sea.

1 Introduction

The Eastern Mediterranean (EM) is a semi-enclosed extremely oligotrophic basin. Due to significant exceeding of evaporation, relative runoff and precipitation, the Mediterranean imports from the North Atlantic upper water with low contents of nutrients (e.g. Siokou-Frangou et al., 2010; Krom et al., 2010; Tanaka et al., 2007, 2011), while exporting nutrients through the deep water outflow. Within the EM, the Levantine Basin (LB) is the most oligotrophic region, with low nutrient and low chlorophyll (LNLC) concentrations, especially during the stratified period (late spring to early autumn) (Berman

BGD
9, 17975–17997, 2012

et al., 1986; Yacobi et al., 1995; Herut et al., 2000; Kress and Herut 2001). The EM nutrient budget (Krom et al., 2004, 2010) shows significant nutrient inputs, mainly N and P, via atmospheric deposition (Herut et al., 1999a, 2002a), while in the northern LB Si inputs are dominated by riverine sources (Koçak et al., 2010).

Despite the basin's ultra oligotrophic nature, the LB coastal areas are often characterized by relatively high concentrations of surficial chlorophyll *a* (Chl) near the coastline, as evident from satellite observations (D'Ortenzio and Ribera d'Alcalà, 2009; Groom et al., 2005). Chlorophyll is a proxy to phytoplankton biomass and this infers on higher nutrient concentrations compared to the open sea waters. Similar elevated Chl levels at sites along the Israeli coast were also recorded by hyper-spectral remote sensing surveys (Herut et al., 1999b, 2002b). Intrusion of these nutrient-enriched coastal waters into the open sea often stimulate local plankton blooms that take the form of distinct mesoscale ($\sim 10-\sim 100$ km) Chl patches stretching from the coast to the open sea for periods of days to months (Barale et al., 2008). The persistence of these widely spread intrusion structures (Fig. 1) suggests to have an important impact on the pelagic LB ecosystem.

Formation of mesoscale Chl patterns often results from horizontal stirring (Martin, 2003) that may be generated by meandering of the surface alongshore currents (Gertman et al., 2010). As recently shown, transport barriers induced by the stirring may control the spatial distribution of phytoplankton, through the formation of dynamical boundaries that prevent mixing between water bodies with different physical and biogeochemical characteristics (Lehahn et al., 2007; Huhn et al., 2012). Multi satellite observations show that such dynamical boundaries may separate between ecological niches that are dominated by different phytoplankton types (d'Ovidio et al., 2010), and can form quasi-isolated planktonic systems that are separated from their surroundings for several months (Lehahn et al., 2011). In addition, it was shown that dynamical boundaries may form barriers and trap passive scalars even at small scales of ~ 1–10 km (Gildor et al., 2009) . This suggests that the coast to open sea intrusions observed in the LB, represent not only transport of coastal waters with their unique

BGD
9, 17975–17997, 2012

characteristics, but also isolated systems that are separated from ambient waters by transport barriers associated with the surface velocity field.

The current study is aimed at characterizing and estimating the possible environmental impacts of coast-to-open sea intrusions on the pelagic water of the LB. We focus on an individual intrusion event that took the form of a distinct Chl patch stretching from the Mediterranean coast of Israel to the open sea (Fig. 2a). This event represents similar long-term ongoing events observed along the coast of Israel and other EM coasts (Fig. 1) We characterized the patch's physical, chemical and biological properties, in comparison to the properties of the waters surrounding it. The strategy for the research was as follows. First, the patch and its transport barriers were identified from analysis of near real time satellite data. Then a high resolution field campaign was launched, covering the area of the patch and its vicinity. The sampling strategy for the campaign was planned and implemented based on satellite-based estimates of the patch extension, and on continuous on-board measurements of surface temperature and fluorescence.

2 Data and methods

2.1 Satellite data

Surface currents were obtained from the AVISO database (http://www.aviso.oceanobs.com/). During the period examined in this study, the distributed global product was a combination of altimetric data from Jason-1&2 and Envisat missions. The dataset was comprised of daily near-real-time sea-level-anomaly data files, gridded on a $1/8^{\circ} \times 1/8^{\circ}$ Mercator grid. This product also included the mean dynamic topography field RioMed (Rio et al., 2007). In the study area, the dataset did not include measurements at distances of less than ~ 10 km from the coastline. Identification of transport barriers was done through extraction of unstable manifolds (also referred to as attracting Lagrangian coherent structures (see Haller and Yuan, 2000)) from the calculation of finite

BGD
9, 17975–17997, 2012

size Lyapunov exponents (FSLE) (Boffetta et al., 2001; d'Ovidio et al., 2004; Lehahn et al., 2007).

Surface Chl and sea surface temperature (SST) were derived from the Moderate Resolution Imaging Spectroradiometer (MODIS) aboard Aqua. The dataset was comprised of 1 km images, obtained from the ocean color data distribution site (http://oceandata.sci.gsfc.nasa.gov/).

2.2 In situ measurements

The cruise was conducted aboard the R/V *Shikmona* on the 22–24 August 2011, when the patch was distinctly evident in satellite images of sea surface chlorophyll (Fig. 2a). We sampled 19 stations that represent the conditions IN and OUT of the patch (Fig. 3; the criterion for defining stations IN and OUT of the patch is described in Sect. 3). In each station continuous profiles of pressure, temperature salinity, dissolved oxygen, and fluorescence were measured using the Sea-Bird SBE 911 plus CTD system, interfaced to a SBE Carousel equipped with twelve, eight liters Niskin bottles. In addition, at 13 stations, water samples for the determination of nutrients, Chl and picophytoplankton were collected using Niskin bottles at four sampling depths: two at the upper mixed layer (surface and base of the mixed layer), one at the minimum salinity layer (Min_{Sal}), and one at the deep chlorophyll maximum (DCM). In addition, continuous measurements of temperature, salinity and Chl-fluorescence of surface waters were performed along the cruise track using an additional CTD and a flow through system.

Duplicate water samples for the determination of nutrients were collected in 15-mL acid-washed plastic scintillation vials and were immediately frozen. Nutrients were determined in the laboratory using a segmented flow Seal Analytical AA-3 system by the methods described by Krom et al., (1991) and Kress and Herut (2001). Duplicate samples of 1.8 cm^3 for picophytoplankton enumeration were fixed immediately upon collection with 20 µl of 25 % glutaraldehyde, retained at room temperature for 10 min, frozen in liquid nitrogen and stored at −80 °C until analysis within 2 months from collection. Before analysis in the laboratory, samples were fast thawed at 37 °C, and excited

BGD
9, 17975–17997, 2012

in a flow cytometer – FACScan Becton Dickinson, fitted with an argon laser (488 nm) for 10 to 15 min or until 30 000 cells were counted (Marie et al., 2005) Taxonomic discrimination was based on: cell side-scatter – a proxy of cell volume; forward scatter – a proxy of cell size; and orange and red fluorescence of phycoerythrin and of Chl (585 nm and 630 nm respectively). Samples for Chl determination were filtered through GF/F filters that were folded, wrapped in aluminum paper and frozen. Chl was measured fluorimetrically following extraction with 95 % acetone (Holm-Hansen et al., 1965). The results were used to calibrate the CTD fluorescence profiles.

3 Results and discussion

The intrusive patch characterized in this work is distinctly identified as a positive Chl concentrations anomaly (Fig. 2a). On average, satellite derived Chl concentrations are $0.16 \pm 0.08\,\mathrm{mg\,m^{-3}}$ within the patch and $0.06 \pm 0.03\,\mathrm{mg\,m^{-3}}$ in the surrounding waters. The patch, which extends from the eastern coastline towards the open sea, covers an overall area of approximately 4000 $\mathrm{km^2}$ (~ 100 km in length and ~ 40 km in width). The lifetime of the patch, deduced from analyzing a sequence of Chl concentrations maps (not shown), is about 45 days (from 30 July to 12 September), a period during which its shape and size vary. The Chl patch overlapps a similar structure of warmer waters (average satellite derived temperature of $28.6 \pm 0.4\,^{\circ}\mathrm{C}$ within the patch vs. $28.2 \pm 0.2\,^{\circ}\mathrm{C}$ in the surrounding waters) in the sea surface temperature field (Fig. 2b).

These patch characteristics are similar to the relatively high Chl and SST in the nearby coastal region. This spatial continuity in high Chl and SST levels suggests that the waters in the patch originate in the coastal area. This hypothesis is strongly supported by the westward direction of surface currents associated with the patch (Fig. 2c). Further examination of the surface currents impact on the properties of the patch was carried out by detecting transport barriers through calculation of FSLE from satellite derived velocity fields (Fig. 2d). More specifically, we focused on the FSLE adjacent to the patch (red and black lines in Figs. 2d and 3, respectively). In accordance with

BGD
9, 17975–17997, 2012

the hypothesis of the patch resulting from westward advection of coastal waters, the adjacent FSLE forms a dynamical "corridor" delimiting the patch from the north and from the south. The southern edge of the patch remarkably coincides with the adjacent FSLE (Fig. 2d), suggesting the latter acts as a dynamic patch boundary (DPB) that separates between the patch and the waters south of it. The closest FSLE to north is found approximately 20 km to the patch's northern edge. This discrepancy can be attributed to insufficient resolution (in space and time) of the satellite altimetry data.

The ability of unstable manifolds derived from FSLE calculation to delimit transport barriers that shape and separate marine systems with distinct physical-biogeochemical properties was recently shown in a number of studies (Lehahn et al., 2007; d'Ovidio et al., 2010; Huhn et al., 2012). Here, this ability is tested through continuous in situ measurements of temperature and fluorescence at three sections across the DPB, which is delimited by the unstable manifold adjacent to the patch southern edge (Fig. 4). In agreement with the notion of unstable manifolds bounding marine systems, the crossing of the DPB (black squares in Fig. 4) is associated with strong fronts in temperature and fluorescence, with both fields going from background (i.e. outside the patch) levels to maximum-patch-levels over short distances of less than 5 km.

The surface properties of the water body associated with the patch (derived from the satellite and continuous in situ datasets), strongly suggest that it can be considered as a dynamically isolated or quasi-isolated system (Lehahn et al., 2011), whose physical, chemical and biological properties are significantly different from those of its surroundings. This view of the patch is further examined by comparing a series of depth profiles in stations IN and OUT of the patch (Fig. 5). The location of the stations (with respect to the patch) was defined objectively according to the location of the fronts in surface fluorescence and temperature (blue stars and red triangles in Fig. 4, for stations IN and OUT of the patch, respectively).

In agreement with previous late summer measurements (D'Ortenzio et al., 2005), the water column is well stratified, with a distinct mixed layer reaching a depth of approximately 25 m (Fig. 5a). Within the mixed layer, water associated with the patch

BGD
9, 17975–17997, 2012

(blue points in Fig. 5) are less dense (24.75–25.5 $kg\,m^{-3}$), less saline (38.9–39.2) and warmer (29–30 °C), than those outside the patch (25.5 $kg\,m^{-3}$, 38.9–39.4 and 28–29 °C, respectively; red points in Fig. 5). For greater depths, water density, salinity and temperature do not exhibit significant differences between waters IN and OUT of the patch. Hence, we deduce that the patch corresponds to a distinct water body whose physical properties differ significantly from those of ambient waters, and that is associated with isolated horizontal transport through the ~ 25 m mixed layer. The low salinity water within the patch most likely originates from a local coastal upwelling due to alongshore current meander. At the surface the water warms quickly due to high salinity stratification inside the patch. Based on previous works, we estimate that the local upwelling occurred in the vicinity of Haifa bay (northeast to the patch), where circulation is disturbed by the complicate topography (Rosentraub and Brenner, 2007).

Further elucidation of the link between the patch properties and horizontal transport by surface currents was obtained by the extraction of satellite derived Chl time series, over 4 regions of interest (ROI) located at equal distances (0.2°) along the patch's main axis (Fig. 6a). For all 4 ROIs, Chl evolution is characterized by a distinct increase in surface chlorophyll concentrations (Fig. 6b). The timing of Chl increase varies between the 4 ROIs, starting near the coast (ROI A), and gradually advancing as the distance from the coast increases. Following the assumption that the patch is driven by horizontal transport of productive coastal waters, the differences in timing (of Chl increase) can be interpreted as the time required for the patch to cover the distances between the ROIs, thus providing a measure to the patch propagation speed. Dividing the distance between the ROIs and timing of chlorophyll increase provides an estimated propagation velocity of approximately 7.4 $km\,d^{-1}$ (~ 0.09 $m\,s^{-1}$), which is in agreement with the velocity of the surface currents (~ 0.1 $m\,s^{-1}$). Considering the described above patch dimensions (~ 40 km width and ~ 25 m depth) and propagation speed, we estimate the outflow volume of coastal water associated with the patch (and responsible to its formation), to be at the order of ~ 0.1 Sv. Though representing a transient short term (~ 10 days) event, this is a remarkable volume flux of water, which is comparable to main EM

BGD
9, 17975–17997, 2012

water pathways, as the mean outflow from the Aegean Sea (e.g. averages of 0.4 Sv for the years 1987–1994 (Nittis et al., 2003), and 0.7 Sv for the years 1988–1993, Rupolo et al., 2003).

The patch is also characterized by a distinct biogeochemical signature. A significant inorganic chemical indicator is the dissolved concentration of silicic acid ($Si(OH)_4$) (Fig. 7a, b). $Si(OH)_4$ concentrations within the patch are higher by 22–35 % than outside of it at the surface and MLD. Inside the patch, $Si(OH)_4$ ranged from 1.3 to 2.2 $\mu mol\,kg^{-1}$ at the surface, and 0.8 to 1.6 $\mu mol\,kg^{-1}$ at MLD. The linear relationship ($R^2 = 0.5$) between $Si(OH)_4$ concentrations and temperature for surface water, represents a conservative behavior of mixing between two end-members, shallow coastal waters, warm and enriched with $Si(OH)_4$, and open sea pelagic water, colder with lower levels of $Si(OH)_4$ (Fig. 8a). No similar signal is identified for $NO_3 + NO_2$ nor for PO_4, whose concentrations were low and similar at all stations (0.5–1.0 $\mu mol\,kg^{-1}$ and close to the detection limit (0.007 $\mu mol\,kg^{-1}$), respectively). As previously shown, a possible source for the anomalously high levels of silicic acid, is discharge of nutrient enriched freshwaters from springs (Weinstein et al., 2006).

Abundance of *Synechococcus* cells at the surface was 2 fold higher inside the patch than outside of it, with maximal abundances at stations 11 and 12 (3.2×10^7 and 2.5×10^7 cells l^{-1}, respectively) (Fig. 7c, d). At the OUT stations *Synechococcus* abundance was low, ranging from 4.9×10^6 to 1.2×10^7 cells l^{-1}, except for surface water of the coastal stations 1 and 8 where high abundances were observed (2.8×10^7 and 2.4×10^7 cells l^{-1}, respectively). The vertical trend in *Synechococcus* abundance remained the same with > 2 fold increase in average cell number at the IN rather than the OUT. *Picoeukaryotes* abundance was higher at the IN patch stations compared to the surroundings by 1.5–2.3 fold throughout all depths sampled (Fig. 7 e, f). This enrichment was also reflected in the significant linear relationship ($R^2 = 0.62$) between *picoeukaryotes* abundance and temperature at the surface and MLD samples (Fig. 8b). Inside the patch, surface picoeukaryotes abundance is relatively constant (~ 1.4×10^6 cells l^{-1}), increasing toward the MLD (station 11, 2.8×10^6 cells l^{-1})

BGD
9, 17975–17997, 2012

and Min_{Sal} (2.7×10^6 cells l^{-1}). *Prochlorococcus* abundance did not show any significant spatial trend, with values ranging from 1.5×10^7 to 1.8×10^7 cells l^{-1} and 3×10^6 to 1×10^7 cells l^{-1} for stations located in and out of the patch, respectively (not shown). It is reasonable to assume that the higher abundance of *Synechococcus and picoeukaryotes* inside the patch was a result of available nitrate and phosphate supplied from the near shore. Their utilization decreased the concentrations in seawater and masked any differences between the IN and OUT waters. The relatively high $Si(OH)_4$ concentration found inside the patch suggests that most of the $Si(OH)_4$ was not utilized and remained in the seawater.

4 Summary and conclusions

In this work we integrated near real time multi satellite datasets and in situ measurements from a high-resolution survey, to characterize physical-biogeochemical properties of a patch stretching from the coast to the open sea, in the Levantine basin of the Eastern Mediterranean. Based on Lagrangian analysis of satellite derived velocity field, and comparison with spatial variations of in situ measured physical and biogeochemical properties, the patch is identified as a semi-enclosed system that is bounded within a ~ 25 m mixed layer and is separated from ambient waters by transport barriers induced by the surface currents. The separation between the patch and its surroundings is expressed by significant differences in a number of physical (the patch is less saline and warmer) and biogeochemical (the patch is richer with silicic acid and chlorophyll, and is more abundant in *Synechococcus* and picoeukaryotes cells) parameters. The anomalous values associated with the patch can originate both in local upwelling introducing waters from below the seasonal thermocline, and in coastal waters that are influenced by terrestrial sources as rivers and submarine groundwater discharges.

These results suggest that horizontal stirring is likely to have an important impact on the ultra-oligotrophic Levantine basin ecosystem, through two main scenarios:

BGD
9, 17975–17997, 2012

1. Transport of nutrients and coastal derived material from near shore area to the open sea. This potential importance is emphasized by the fact that the patch is associated with a remarkable westward volume flux (~ 0.1 Sv), and by the fact that similar structures appear regularly at different locations around the basin's periphery. Furthermore, since coastal environments are globally highly productive areas (Chavez and Smith, 1995), the suggested impact of horizontal stirring is likely to be important at the coast-open sea interface around the globe, especially at oligotrophic areas.

2. Formation of local niches that are separated from their surrounding by transport barriers, and are thus subject to different dynamics. As recently shown by d'Ovidio et al. (2010), such fluid dynamical niches may sustain different planktonic communities, and can play a key role in the dynamics and maintenance of planktonic biodiversity in the interface between the coastal area and the open sea.

Finally, we note that the accurate detection of transport barriers from near real time satellite altimetry data, together with the proven ability to plan and execute a high resolution sampling strategy, provide a promising framework for efficient rapid response in cases of pollution events in the interface between coast and the open sea.

Acknowledgements. This research was funded by the Israeli Ministry of Science and Technology (MOST 3-6490). The authors acknowledge NASA access to MODIS-Aqua data. The altimeter products were produced by Ssalto/Duacs and distributed by Aviso with support from the Centre National d'Études Spatiales. We are grateful to the crew of the R/V *Shikmona* and the research assistants of the Marine Chemistry Department at IOLR for their help at sea and in the laboratory. Eyal Heifetz is grateful for the Rossby Visiting Fellowship of the International Meteorological Institute (IMI) of Sweden. All figures in this paper received their final touch by using Inkscape, an open source vector graphics editor.

BGD
9, 17975–17997, 2012

References

Barale, V., Jaquet, J.-M., and Ndiaye, M.: Algal blooming patterns and anomalies in the Mediterranean Sea as derived from the SeaWiFS data set, Remote Sens. Environ., 112, 3300–3313, 2008.

Berman, T., Azov, Y., Schneller, A., Walline, P., and Townsend, D. W.: Extent, transparency, and phytoplankton distribution of the neritic waters overlying the Israeli coastal shelf, Oceanol. Acta, 9, 439–447, 1986.

Boffetta, G., Lacorata, G., Redaelli, G., and Vulpiani, A.: Detecting barriers to transport: a review of different techniques, Physica D, 159, 58–70, 2001.

Chavez, F. and Smith, S.: biological and chemical consequences of open ocean upwelling, Environ. Sci. Res. Rep., 18, 149–170, 1995.

D'Ortenzio, F. and Ribera d'Alcalà, M.: On the trophic regimes of the Mediterranean Sea: a satellite analysis, Biogeosciences, 6, 139–148, doi:10.5194/bg-6-139-2009, 2009.

D'Ortenzio, F., Iudicone, D., De Boyer Montegut, C., Testor, P., Antoine, D., Marullo, S., Santoleri, R., and Madec, G.: Seasonal variability of the mixed layer depth in the Mediterranean Sea as derived from in situ profiles, Geophys. Res. Lett., 32, 2–5, 2005.

D'Ovidio, F., Fernández, V., Hernández-García, E., and López, C.: Mixing structures in the Mediterranean Sea from finite-size Lyapunov exponents, Geophys. Res. Lett., 31, 1–7, 2004.

D'Ovidio, F., De Monte, S., Alvain, S., Dandonneau, Y., and Lévy, M.: Fluid dynamical niches of phytoplankton types., P. Natl. Acad. Sci. USA, 107, 18, 366–370, doi:10.1073/pnas.1004620107, 2010.

Gertman, I., Goldman, R., Rosentraub, Z., Ozer, T., Zodiatis, G., Hayes, D., and Poulain, P.- M.: Generation of Shikmona anticyclonic eddy from an alongshore current, Rapp. Comm. Int. Mer Medit. (CIESM Congress Proceedings), 39, p. 117, 2010.

Gildor, H., Fredj, E., Steinbuck, J., and Monismith, S.: Evidence for submesoscale barriers to horizontal mixing in the ocean from current measurements and aerial-photographs, J. Phys. Oceanogr., 39, 1975–1983, doi:10.1175/2009JPO4116.1, 2009.

Groom, S., Herut, B., Brenner, S., Zodiatis, G., Psarra, S., Kress, N., Krom, M. D., Law, C. S., and Drakopoulos, P.: Satellite-derived spatial and temporal biological variability in the Cyprus Eddy, Deep Sea Res., 52, 2990–3010, 2005.

Haller, G. and Yuan, G.: Lagrangian coherent structures and mixing in two-dimensional turbulence, Physica D, 147, 352–370, doi:10.1016/S0167-2789(00)00142-1, 2000.

BGD
9, 17975–17997, 2012

Herut, B., Krom, M., Pan, G., and Mortimer, R.: Atmospheric input of nitrogen and phosphorus to the se Mediterranean: sources, fluxes and possible impact, Limnol. Oceanogr., 44, 1683–1692, 1999a.

Herut, B., Tibor, G., Yacobi, Y. Z., and Kress, N.: Synoptic measurements of chlorophyll *a* and suspended particulate matter in a transitional zone from polluted to clean seawater utilizing airborne remote sensing and ground measurements, Haifa bay (se Mediterranean), Mar. Poll Bull., 38, 762–772, 1999b.

Herut, B., Almogi-Labin, A., Jannink, N., and Gertmann. I.: Seasonal dynamics of nutrient and chlorophyll *a* concentrations on the se Mediterranean shelf-slope, Oceanol. Acta, 23, 771–782, 2000.

Herut, B., Collier, R., and Krom, M. D.: The role of dust in supplying N and N to the se Mediterranean, Limnol. Oceanogr., 47, 870–878, 2002a.

Herut, B., Kress, N., and Tibor, G.: The use of hyper-spectral remote sensing in compliance monitoring of water quality (phytoplankton and suspended particles) at "hot spot" areas (Mediterranean coast of Israel), Fresenius Environ. Bull., 11, 782–787, 2002b.

Holm-Hansen, O., Lorenzen, C. J., Holmes, R. W., and Strickland, J. D. H.: Fluorometric determination of chlorophyll, J. Conseil., 30, 3–15, 1965.

Huhn, F., von Kameke, A., Perez-Munuzuri, V., Olascoaga, M. J., and BeronVera, F. J.: The impact of advective transport by the South Indian Ocean countercurrent on the madagascar plankton bloom, Geophys. Res. Lett., 39, L06602, doi:10.1029/2012GL051246, 2012.

Koçak, M., Kubilay, N., Tuğrul, S., and Mihalopoulos, N.: Atmospheric nutrient inputs to the northern levantine basin from a long-term observation: sources and comparison with riverine inputs, Biogeosciences, 7, 4037–4050, doi::0.5194/bg-7-4037-2010, 2010.

Kress, N. and Herut, B.: Spatial and seasonal evolution of dissolved oxygen and nutrients in the Southern Levantine Basin (Eastern Mediterranean Sea): chemical characterization of the water masses and inferences on the N : P ratios, Deep Sea Res., 48, 2347–2372, 2001.

Krom, M. D., Brenner, S., Kress, N., and Gordon, L.: Phosphorus limitation of primary productivity in the Eastern mediterranean sea, Limnol. Oceanogr., 36, 424–432, 1991.

Krom, M. D., Herut, B., and Mantoura, R. F. C.: Nutrient budget for the Eastern Mediterranean: implications for phosphorus limitation, Limnol. Oceanogr., 49, 1582–1592, 2004.

Krom, M. D., Emeis, K.-C., and Van Cappellen, P.: Why is the Eastern Mediterranean phosphorus limited?, Prog. Oceanog., 85, 236–244, 2010.

BGD
9, 17975–17997, 2012

Lehahn, Y., D'Ovidio, F., Lévy, M., and Heifetz, E.: Stirring of the northeast Atlantic spring bloom: a Lagrangian analysis based on multisatellite data, J. Geophys. Res., 112, C08005, doi:10.1029/2006JC003927, 2007.

Lehahn, Y., D'Ovidio, F., Lévy, M., Amitai, Y., and Heifetz, E.: Long range transport of a quasi isolated chlorophyll patch by an Agulhas ring, Geophys. Res. Lett., 38, 1–6, 2011.

Marie, D., Simon, N., and Vaulot, D.: Phytoplankton cell counting by flow cytometry, in: Algal Culturing Techniques, edited by: Andersen, R. A., Academic Press, San Diego, CA, USA, 253–267, 2005.

Martin, A. P.: Phytoplankton patchiness: the role of lateral stirring and mixing, Prog. Oceanogr., 57, 125–174, 2003.

Nittis, K., Lascaratos, A., Theocharis, A.: Dense water formation in the Aegean Sea: numerical simulations during the Eastern Mediterranean Transient, J. Geophys, Res., 108, C9, PBE 21, doi:10.1029/2002JC001352, 2003.

Rio, M., Poulain, P., Pascual, A., Mauri, E., Larnicol, G., and Santoleri, R.: A mean dynamic topography of the Mediterranean Sea computed from altimetric data, in situ measurements and a general circulation model, J. Mar. Syst., 65, 484–508, doi:10.1016/j.jmarsys.2005.02.006, 2007.

Rosentraub, Z. and Brennerb, S.: Circulation over the southeastern continentalshelf and slope of the Mediterranean Sea: direct current measurements, winds, and numerical model simulations, J. Geophy. Res., 112, C1 1001, doi:10.1029/2006JC003775, 2007.

Rupolo, V., Marullo, S., and Iudicone, D.: Eastern Mediterranean transient studied with Lagrangian diagnostics applied to a Mediterranean OGCM forced by satellite SST and ECMWF wind stress for the years 1988–1993, J. Geophys. Res., 108, C9, doi:10.1029/2002JC001636, 2003.

Schlitzer, R.: Ocean Data View, http://odv.awi.de, 2011.

Siokou-Frangou, I., Christaki, U., Mazzocchi, M. G., Montresor, M., Ribera d'Alcalà, M., Vaqué, D., and Zingone, A.: Plankton in the open Mediterranean Sea: a review, Biogeosciences, 7, 1543–1586, doi:10.5194/bg-7-1543-2010, 2010.

Tanaka, T., Zohary, T., Krom, M. D., Law, C. S., Pitta, P., Psarra, S., Rassoulzadegan, F., Thingstad, T. F., Tselepides, A.,Woodward, E. M. S., Fonnes Flaten, G. A., Foss Skjoldal, E., Zodiatis, G.: Microbial community structure and function in the levantine basin of the Eastern Mediterranean, Deep Sea Res., 54, 1721–1743, 2007.

BGD
9, 17975–17997, 2012

Tanaka, T., Thingstad, T. F., Christaki, U., Colombet, J., Cornet-Barthaux, V., Courties, C., Grattepanche, J.-D., Lagaria, A., Nedoma, J., Oriol, L., Psarra, S., Pujo-Pay, M., and Van Wambeke, F.: Lack of P-limitation of phytoplankton and heterotrophic prokaryotes in surface waters of three anticyclonic eddies in the stratified Mediterranean Sea, Biogeosciences, 8, 525–538, doi:10.5194/bg-8-525-2011, 2011.

Weinstein, Y., Less, G., Kafri, U., and Herut, B.: Submarine groundwater discharge in the Southeastern Mediterranean (Israel), preliminary results, Radioactiv. Environ., 8, 360–372, 2006.

Yacobi, Y., Zohary, T., Kress, N., Hecht, A., Robarts, R., Waiser, M., Wood, A., and Li, W.: Chlorophyll distribution throughout the Southeastern Mediterranean in relation to the physical structure of the water mass, J. Mar. Syst., 6, 179–190, doi:10.1016/0924-7963(94)00028-A, 1995.

BGD

9, 17975–17997, 2012

Intrusion of coastal waters into the pelagic Eastern Mediterranean

S. Efrati et al.

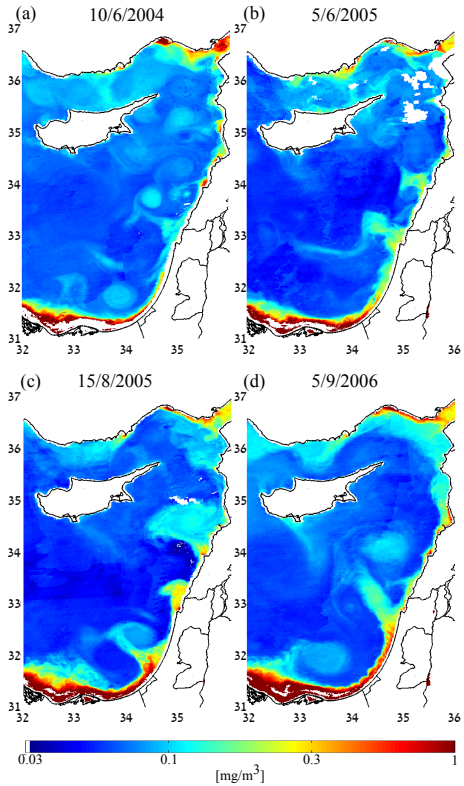

Fig. 1. Distribution patterns of surface chlorophyll *a* in the Levantine Basin of the Eastern Mediterranean, emphasizing the abundance of mesoscale structure extending from the coastal area to the open sea at four different dates. To reduce the area masked by clouds, the images are composed of 8 consecutive days. Throughout the manuscript, surface chlorophyll *a* and temperature images are derived from MODIS-Aqua 1 km data.

BGD
9, 17975–17997, 2012

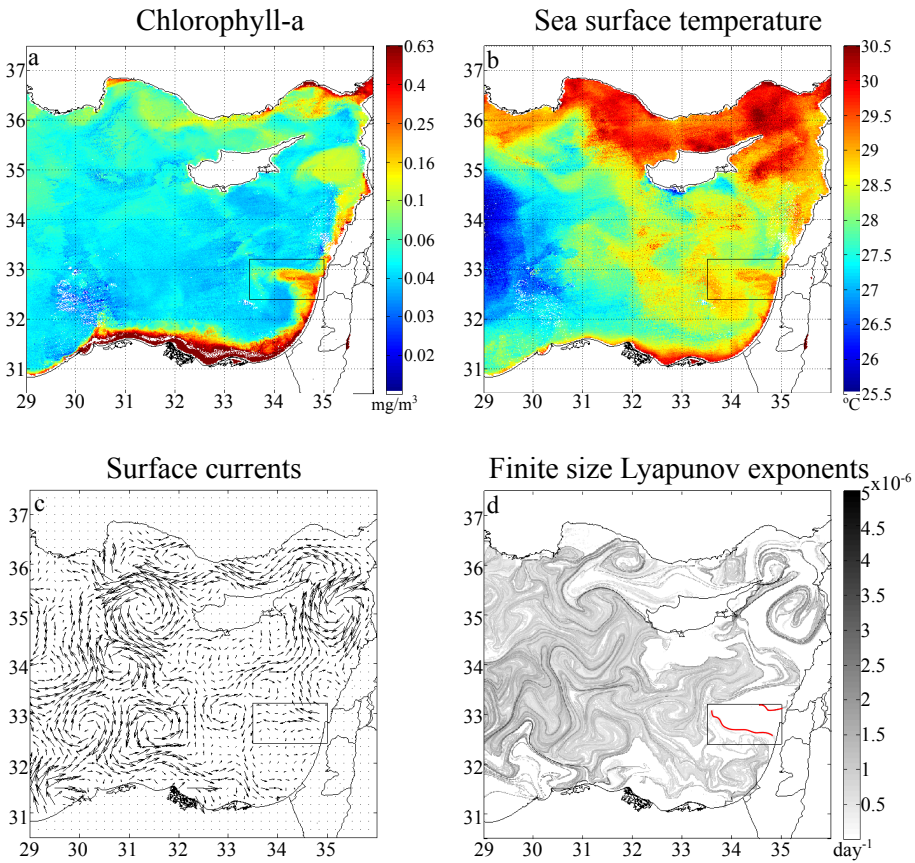

Fig. 2. Satellite derived maps of the Levantine Basin of the Eastern Mediterranean **(a)** chlorophyll *a* concentrations; **(b)** sea surface temperature; **(c)** surface currents and **(d)** finite size Lyapunov exponents, from 22 August 2011. The boxes mark the area shown in Fig. 3. The red lines in panel **(d)** highlight the unstable manifolds constraining the patch from the north and from the south (see text).

BGD
9, 17975–17997, 2012

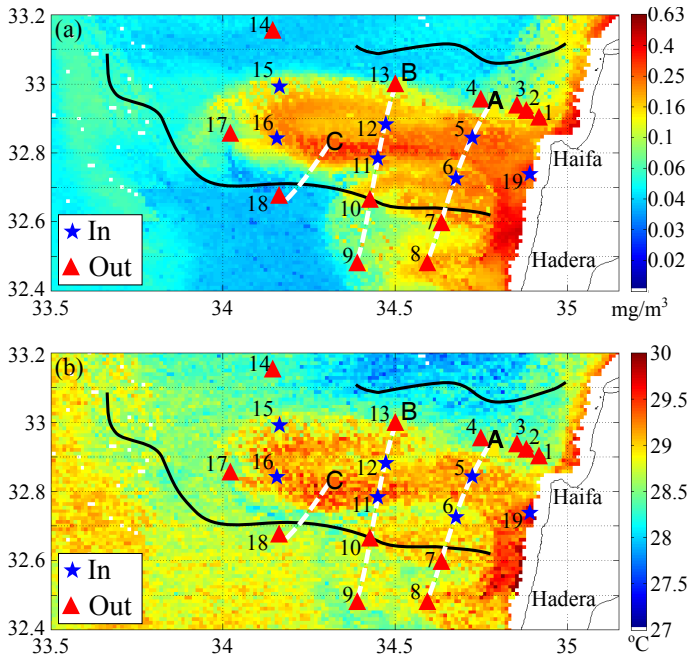

Fig. 3. Sea surface **(a)** chlorophyll *a* and **(b)** temperature associated with the intrusive patch observed on the 22 August 2011. Solid black lines mark the unstable manifolds constraining the patch from the north and from the south. Dashed white lines mark the sections presented in Fig. 4. Blue stars and red triangles represent the locations of sampling stations IN and OUT of the patch, respectively (location of the stations with respect to the patch is defined according the sections in Fig. 4). Numbers denote stations names. The letters A, B and C mark the corresponding to sections delimited respectively in Fig. 4a–c. The black lines highlight the unstable manifolds constraining the patch from the north and from the south.

BGD
9, 17975–17997, 2012

Intrusion of coastal waters into the pelagic Eastern Mediterranean

S. Efrati et al.

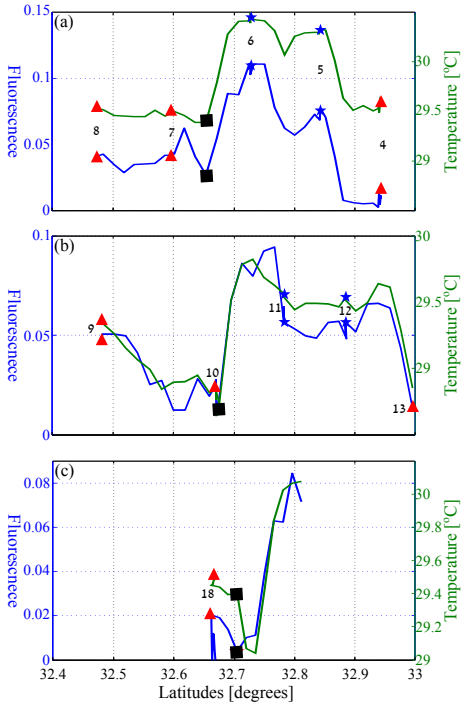

Fig. 4. In situ measured surface temperature (green) and fluorescence (blue) along three meridional sections orthogonal to the patch's main axis (white-dashed lines and corresponding letters in Fig. 3). Blue stars and red triangles mark the locations of sampling stations IN and OUT of the patch, respectively. Numbers denote station names. The black square marks intersection with the southern dynamic patch boundary (DPB), associated with the strong unstable manifold adjacent to the patch southern edge. Note the change in scale between the different panels.

BGD
9, 17975–17997, 2012

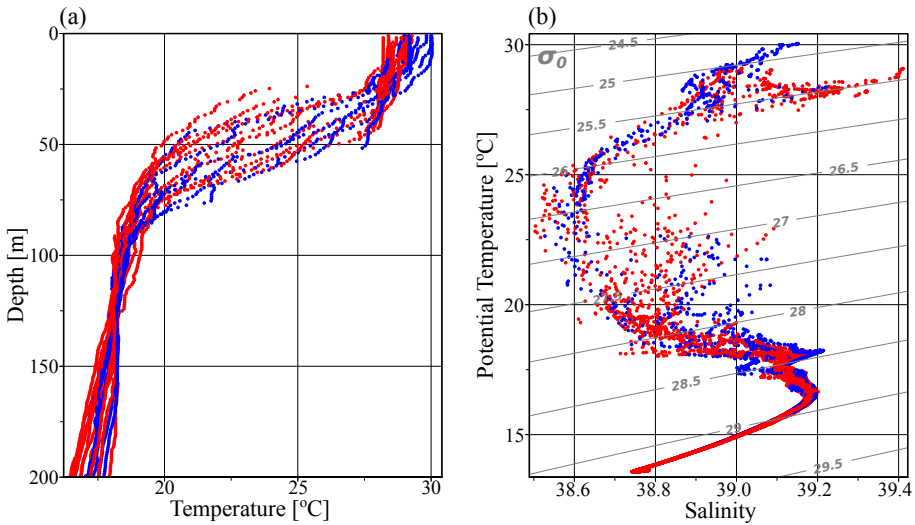

Fig. 5. (a) Vertical profiles of temperature and **(b)** T-S diagram, for stations IN (blue) and OUT (red) of the patch (see Fig. 3 for station locations). Figure was made using Ocean Data View (Schlitzer, 2011).

BGD
9, 17975–17997, 2012

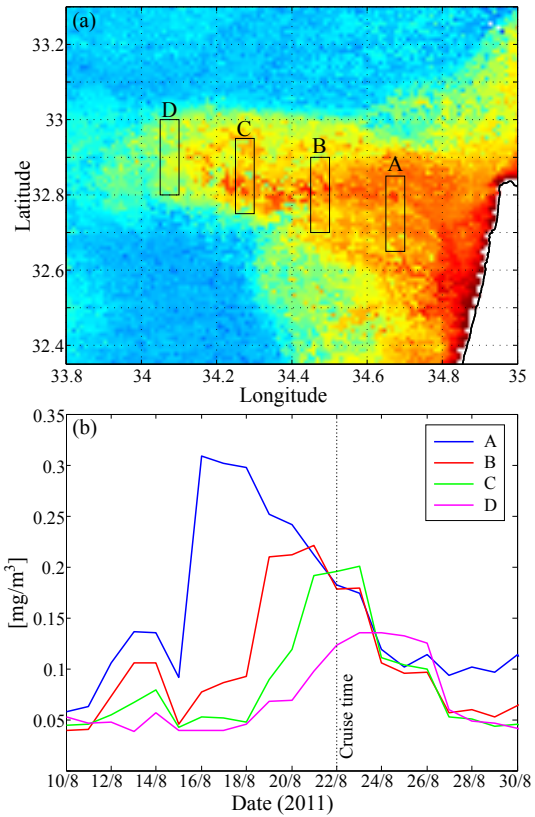

Fig. 6. (a) Black boxes mark the locations of regions of interest (ROI) along the patch's main axes, used for extracting the time series in panel **(b)**. The ROIs are superimposed on a satellite derived chlorophyll map showing the patch's extension. **(b)** Temporal evolution of surface chlorophyll concentrations at the 4 regions of interest along the patch's main axis.

BGD
9, 17975–17997, 2012

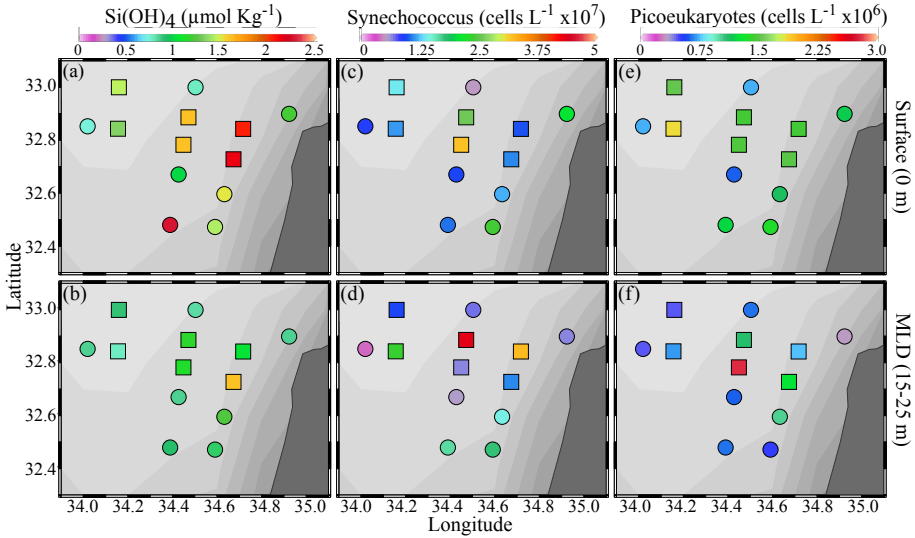

Fig. 7. Spatial distribution of **(a, b)** $Si(OH)_4$ concentrations; **(c, d)** *Synechococcus* and **(e, f)** picoeukaryotes abundance at the surface (upper panels) and mixed layer depth (lower panels). Squares and circles mark stations located IN and OUT of the patch, respectively (see Fig. 3 for station numbers). Figure was made using Ocean Data View (Schlitzer, 2011).

BGD
9, 17975–17997, 2012

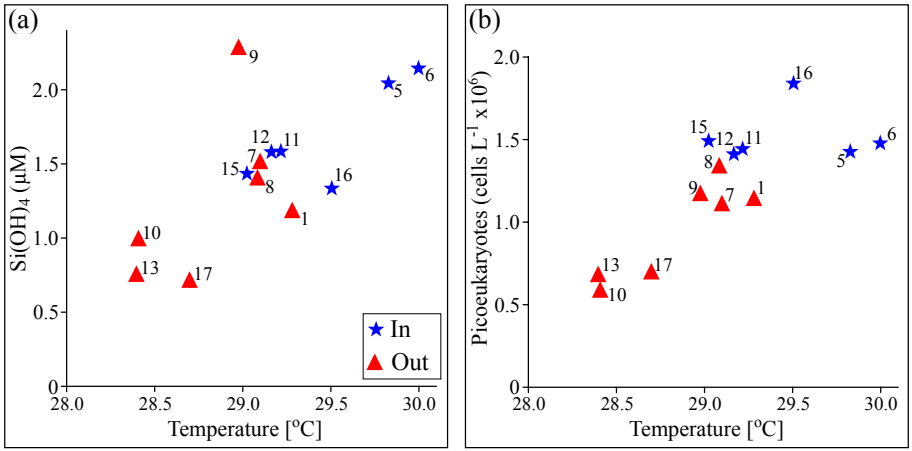

Fig. 8. Relationships between temperature and **(a)** dissolved silicic acid ($Si(OH)_4$) concentrations and **(b)** abundance of *picoeukaryotes* cells at surface waters from stations IN and OUT of the patch.

BGD
9, 17975–17997, 2012